SIMULATION OF THE THREE-DIMENSIONAL BEHAVIOR OF AN UNSTEADY LARGE BUBBLE NEAR A STRUCTURE

Georges L. Chahine[a] and Thomas O. Perdue
DYNAFLOW, Inc.
10422 Mountain Quail Road
Silver Spring, Maryland 20901

ABSTRACT

In most practical applications existing bubble dynamics models, either spherical or axisymmetric, are only more or less appropriate approximations. In this paper we will describe an on-going project which considers the fully three-dimensional bubble dynamics problem. The interaction between a growing, deforming and collapsing bubble near a boundary is simulated numerically using a Boundary Integral Method. The example of large bubble dynamics near a solid flat plate in a gravity field is considered. The plate orientation significantly influences the 3-D bubble shape and behavior. The flow field due to the bubble dynamics is considered to be potential. To initialize the computations, the bubble is taken to be very small and spherical. From there on, no additional assumptions are imposed and the bubble surface is free to move under the influence of the pressure field, inertia forces, and the presence of body forces and a nearby wall. The presence of gas inside the bubble is accounted for using a polytropic law of behavior and surface tension is included in the model. This paper presents the method, addresses the numerical difficulties and shows the influence of the problem geometry on the bubble dynamics.

INTRODUCTION

Bubble dynamics has been the subject of much attention since the end of the last century. However, nonspherical bubble dynamics, as well as interaction between bubbles, and between bubbles and neighboring complex boundaries have received much less attention due to the complexity of the nonspherical free boundary problem involved. In recent years the study of bubble dynamics for cavitation erosion problems has focused on bubble behavior near solid boundaries. Blake and Gibson[1] give a very fine overview of all facets of this work. Concerning the modelling of the phenomena, several analytical and numerical methods have been used. To quote a few: a Finite Difference Method was used by Plesset and Chapman[2]; a Variational Principle Method, by Shima and Nakajima[3]; an Asymptotic Expansion Method by Chahine and Bovis[4]; and Chahine and Liu[5]; a Boundary Element Method by Guerri, Luca and Prosperetti[6], etc... these studies were, however, limited to an axisymmetric configuration.

One of the numerical methods that has proven to be very efficient in solving this type of free boundary problem is the Boundary Integral Method. Guerri, et al. and Blake, et al.[7] used this method in the solution of axisymmetric problems of bubble growth and/or collapse near rigid boundaries. However, there are many cases which cannot be handled with an axisymmetric model and require a three-dimensional treatment. In this paper, such a three dimensional numerical model is developed to account for the growth and collapse of a buoyant vapor and gas bubble near boundaries. Buoyancy effects are included to allow the simulation of large bubbles such as those generated by underwater explosions. The three-dimensionality of

---

[a] also Research Professor, Department of Mechanical Engineering, Johns Hopkins University, Baltimore MD.

the problem arises from orienting the rigid boundary arbitrarily relative to the direction of gravity. In general, there is no axis of symmetry, and the entire bubble surface must be considered.

In this paper we present an outline of the model, the problem formulation, the numerical difficulties and the method of solution. We then present the results of a systematic study of bubble behavior in the presence of a solid plane wall at different orientations relative to gravity, and at different distances from the wall. The detailed mathematical expressions involved are very cumbersome and are kept to a minimum. The interested reader is referred to Perdue[8] and Chahine, Perdue and Tucker[9] for more detailed descriptions and expansions.

PROBLEM FORMULATION

It has been shown in earlier studies that due to the relatively large velocities associated with underwater explosion and cavitation bubbles (high Reynolds numbers) viscosity has no appreciable effects on the growth and collapse of bubbles in water. Also, since throughout most of the life of the bubble, the motion of the bubble wall is relatively slow compared to the speed of sound in water, compressibility effects can be ignored. This is valid shortly after bubble inception and until its latest collapse phase. These assumptions, classical in bubble dynamics studies, result in a flow that is potential and satisfies the Laplace equation,

$$\nabla^2 \Phi = 0, \tag{1}$$

where Φ is the velocity potential.

The solution must in addition satisfy boundary conditions at infinity, at the bubble wall and at the boundaries of the submerged body in contact with the fluid. In a fixed reference system of axes centered, for instance, at the initial center of the bubble, the velocity potential at infinity is zero. This condition can be written

$$lim_{\overline{X} \to \infty} \Phi = 0, \tag{2}$$

where $\overline{X}$ is the vector position for a field point P. At all moving surfaces (such as the bubble surface or a moving nearby boundary) an identity between fluid velocities normal to the boundary and the normal velocity of the boundary is to be satisfied. At the bubble-liquid interface, the normal velocity of the moving bubble wall must equal the normal velocity of the fluid, or,

$$\nabla \Phi \cdot \mathbf{n} = \mathbf{V}_s \cdot \mathbf{n}, \tag{3}$$

where $\mathbf{n}$ is the local unit vector normal to the bubble surface and $\mathbf{V}_s$ is the local velocity vector of the moving surface. For a solid stationary boundary, as considered in the examples presented below,

$$\nabla \Phi \cdot \mathbf{n} = 0 \tag{4}$$

For a plane wall, this condition is met exactly by including an image bubble in the computation of the potential and its normal derivative over the bubble surface.

The bubble is assumed to contain noncondensible gas as well as a vapor of the surrounding liquid. The pressure within the bubble at any given time is considered to be the sum of the partial pressures of the noncondensible gases, P_g, and the vapor, P_v, inside the bubble. Vaporization of the liquid is assumed to be fast enough so that the vapor pressure remains constant throughout the simulation and equal to the equilibrium vapor pressure at the ambient liquid temperature. To the contrary, gas diffusion does not have time to occur and the noncondensible gases are assumed to have a polytropic behavior, PV^k = constant, where V is the bubble volume and k is the polytropic constant varying from $k = 1$ for isothermal behavior to $k = 1.4$ for adiabatic conditions.

The pressure at the exterior of the bubble surface, P_L, can be obtained at any time from the following pressure balance expression:

$$P_L = P_v = P_{g_o} \left(\frac{V_o}{V}\right)^k - C\sigma \tag{5}$$

where P_{g_o} and V_o are the initial gas pressure and volume respectively, σ is the surface tension, C is the local curvature of the bubble, and V is the instantaneous value of the bubble volume. P_{g_o} and V_o are known quantities at t=0.

At the beginning of the simulation, the bubble is assumed to be spherical. This approximation is valid as long as the chosen initial bubble size is sufficiently small and the amount of time elapsed since the bubble inception is very short so as to neglect any interaction with the wall. The initial velocity potential of the flow field is then due to a point source of intensity $4\pi R^2 R$ The potential at the bubble wall then becomes

$$\phi_o = -R_o R_o \tag{6}$$

where R_o and R_o are the initial radius and wall velocity of the spherical bubble. The initial wall velocity can be obtained from integrating the Rayleigh-Plesset equation with respect to time (see for instance Chahine[10] or Blake and Taib[7]), using $R = 0$ when $R = R_{max}$. In doing so, one obtains two solutions depending on whether the polytropic constant is greater than or equal to one. For the case where $k > 1$, the following equation is obtained for R_o,

$$\dot{R}_0^2 = \frac{2}{\rho} \frac{P_g}{3(1-k)} \left\langle 1 - \alpha_m^{3k-3} \right\rangle + \frac{P_v + P_a}{3} \left\langle 1 - \alpha_m^{-3} \right\rangle - \frac{\sigma}{R} \left\langle 1 - \alpha_m^{-2} \right\rangle \tag{7}$$

where ρ is the liquid density, $\alpha_m = R_o / R_{max}$, R_{max} being the maximum radius attainable by the bubble in an infinite medium: $k = 1.4$ was used in the results given below.

METHOD OF SOLUTION

The three-dimensional Boundary Integral Method chosen for this problem is based on Green's equation which effectively reduces by one the dimension of the problem. If the velocity potential, Φ, and its normal derivatives are known on the fluid boundaries (points M) and Φ satisfies the Laplace equation as specified in Equation (1), then Φ can be determined anywhere in the domain of the fluid (field points P). This can be written:

$$\iint_s \left[\frac{-\delta\phi}{\delta n} \cdot \frac{1}{|MP|} + \phi \frac{\delta}{\delta n} \left(\frac{1}{|MP|} \right) \right] ds = a\,\pi\phi\,(P) \tag{8}$$

where a is positive and defined as follows:

$a = 4$, if P is a point in the fluid,

$a = 2$, if P is a point on a smooth surface, and

$a < 4$, if P is a point at a sharp corner of the surface.

If the field point P is selected to be on the surface of the bubble or its image, then a closed set of equations can be obtained and used at each timestep to solve for values of $\partial\Phi/\partial$ (or Φ) assuming that all values of Φ (or $\partial\Phi/\partial n$) are known at the preceding step.

To solve Equation (8) numerically, it is necessary to discretize the bubble into panels, perform the integration over each panel, and then sum up the contributions to complete the integration over the entire bubble surface. To do this, the initially spherical bubble is discretized into a geodesic shape with flat, triangular panels. This allows for a rather even initial distribution of nearly equal-sized panels. In the numerical code developed, the fineness of the grid can be controlled relatively easily by prescribing the frequency of subdivision of basic triangles of an icosahedron. With the discretized surface, Equation (8) becomes a set of N equations (N is the number of discretization nodes) of index i of the type:

$$\sum_j \left(\frac{\delta\phi}{\delta n} \cdot A_{ij} \right) = \sum_j \left(\delta_j\, B_{ij} \right) - a\pi\phi_i \tag{9}$$

where A_{ij} and B_{ij} are elements of matrices which correspond numerically to the integrals given in Equation (8). For this discretized problem, the solution is more accurate, and stability is improved, when $\alpha\pi$ is taken at each node to be the solid angle under which the fluid is "seen" from the particular node. The computation of this solid angle is performed at each node and at each time step.

To evaluate the integrals in Equation (8) over any single panel, a transformation from cartesian coordinates to an oblique coordinate system (ζ, η) is made (see Figure 1). Then, by assuming a linear variation of the potential and its normal derivative over the panel, the following expressions can be written for Φ and $\partial\Phi/\partial n$ at any point M on the panel ABC:

$$\Phi(M) = (1-\zeta-\eta)\,\Phi(A) + \zeta\Phi(B) + \eta\Phi(C),$$

$$\frac{\delta\phi}{\delta n}(M) = (1-\zeta-\eta)\frac{\delta\phi}{\delta n}(A) + \zeta\frac{\delta\phi}{\delta n}(B) + \eta\frac{\delta\phi}{\delta n}(C) \qquad (10).$$

In this manner, both Φ and $\partial\Phi/\partial n$ are continuous over the bubble surface and are expressed as a function of the values at the nodal points which define the particular panel. Obviously higher order expansions in powers of ζ and η are conceivable, and would improve accuracy at the expense of additional analytical and numerical computation times. These expansions were not considered in this study. The introduction of the oblique coordinates significantly reduce the complexity of the integrations.

The two integrals in Equation (8) can be evaluated analytically and the resulting expressions, very long and complicated warrant a publication on their own. The complete derivations and results can be found in Perdue[8] and Chahine et al.[9], and are available upon request from the authors. These expressions are generally valid for any panel ABC relative to any node P where P is not on the panel. When the field point P is on the panel over which the integration is being performed, the integrals become singular and warrant special treatment, but can still be evaluated analytically. These singular integrals can be evaluated numerically, but we have instead selected to obtain exact analytical expressions.

In order to proceed with the computation of the bubble dynamics several quantities appearing in the above boundary conditions need to be evaluated at each time. The bubble volume presents no particular difficulties, while the unit normal vector, the local surface curvature and the local tangential velocity at the bubble interface need further development. The curvature of the bubble surface is obtained by first computing a local bubble surface three-dimensional fit, $f(x,y,z) = 0$. The unit normal at a node can then be expressed as:

$$\mathbf{n} = \pm\,\nabla f / |\nabla f| \qquad (11).$$

The appropriate sign is chosen to insure that the normal is always directed toward the fluid. The local curvature is then computed by

$$C = \nabla\cdot\mathbf{n} \qquad (12).$$

To obtain the total fluid velocity at any point on the surface of the bubble, the tangential velocity, $\mathbf{V}_t$, must be computed at each node in addition to the normal velocity, $\partial\Phi/\partial n$. This is also done using a local surface fit to $\Phi_l = g(x,y,z)$. Taking the gradient of this function at the particular node in question and eliminating any normal component of velocity appearing in this gradient gives a good approximation for the tangential velocity. Practically, a second degree equation for the local surface around node N at time t was selected. For instance, for an equation such as:

$$a_1z^2 + a_2z + a_3y^2 + a_4y + a_5x^2 + a_6x + a_7 = 0 \qquad (13)$$

seven parameters a_i have to be determined to obtain the local surface fit equation. This was obtained by using the coordinates of the node of interest, N, and six selected nodes around it and solving the resulting set of 7x7 linear equations. The six extra nodes were selected randomly from a matrix associating to each node all the nodes located on the two immediate rows of nodes surrounding it. A random number generating function was used to select the six needed nodes. In order to reduce errors, the procedure was repeated at least five times, eliminating choices that produced a singular or degenerated system of linear equations. The results were then averaged using the five answers. A similar approach was used to generate the function $g(x,y,z)$ at each node N and time t. Once f and g are determined, the sought variables, C, $\mathbf{n}$ and $\mathbf{V}_t$, are determined using the analytical expressions (11) and (12), and the following expression for $\mathbf{V}_t$:

$$\mathbf{V}_t = \nabla \Phi_t \, x \, \mathbf{n} \qquad (14).$$

With the problem initialized and the velocity potential known over the surface of the bubble, an updated value of $\partial\Phi/\partial n$ can be obtained by performing the integrations outlined above and solving the corresponding matrix equation. The unsteady Bernoulli equation can then be used to solve for $D\Phi/Dt$, the total material derivative of Φ, (using $\mathbf{V}_S = \nabla\Phi$),

$$\frac{D\phi}{Dn} = \frac{\delta\phi}{\delta n} + |\nabla\phi|^2 = \frac{P_a - P_L}{\rho} - \rho g z + \frac{1}{2}|\nabla\phi|^2 \qquad (15).$$

$D\Phi/Dt$ provides the time variations of Φ at any node which is followed during its motion with the fluid. Using an appropriate timestep all values of Φ on the bubble surface can be updated using Φ at the preceding time step and $D\Phi/Dt$.

From our experience, the best choice was based on the ratio between the minimum size of panel sides, l_{min}, and the maximum node velocity, V_{max}:

$$dt = l_{min} / V_{max} \qquad (16)$$

This choice has the great advantage of constantly adapting the timestep, by refining it at the end of the collapse, and increasing it during the slow bubble size variation period. An additional advantage is the prevention of surface "folding" in the latest phases of the collapse and instability enhancement. New coordinate positions of the nodes can then be obtained using the position of the previous time step and the displacement $\partial\Phi/\partial n.\mathbf{n} + V_t.\mathbf{e}_t$ where $\mathbf{e}_t$ is the unit tangent vector, $\mathbf{e}_t = \mathbf{V}_t / |\mathbf{V}_t|$. This time stepping procedure is repeated throughout the bubble growth and collapse, resulting in a fairly complete shape history of the bubble.

The major emphasis of this paper is on the growth and collapse of a bubble near an infinite flat rigid boundary. The algorithm is, however, capable of handling the bubble interaction with nearly any structure geometry. For the infinite flat plate, an image bubble is added to satisfy the boundary condition (4). Thus, the integrations must be carried out over two identical bubble shapes, though the symmetry between them allows for some significant reduction in calculations and computation times. For other cases, the adjacent structure is discretized as well and the integrations are performed over all boundaries with solutions obtained for all nodes (see examples in Chahine et al.[9]).

COMPUTATIONAL RESULTS AND DISCUSSION

Before considering the complex cases of interest to this study the numerical code was tested against existing numerical codes in the literature which are relatively simple. The collapse of a spherical bubble has been extensively studied, and an "exact" analytical-numerical solution exists by numerical integration of the well-known second degree differential equation; the Rayleigh-Plesset equation. In Figure 2, we compare the results of the present numerical code with the "exact" solution for increased degrees of mesh refinement, or discretization frequency. Only the first frequency discretization (12 nodes) shows a significant error on the bubble period (more than 7 percent). The second frequency (42 nodes) and third frequency (92 nodes) show errors of 1.8 and 0.6 percent respectively, while frequencies four (162 nodes) and five (252 nodes) show errors less than 0.14 percent and 0.05 percent respectively. The four frequency discretization was selected for most of the runs shown below.

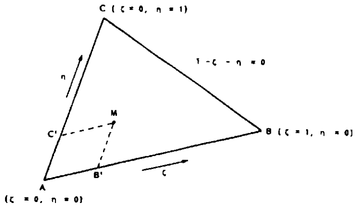

FIGURE 1 - NORMALIZED OBLIQUE COORDINATES ζ, η, ONPANEL ABC

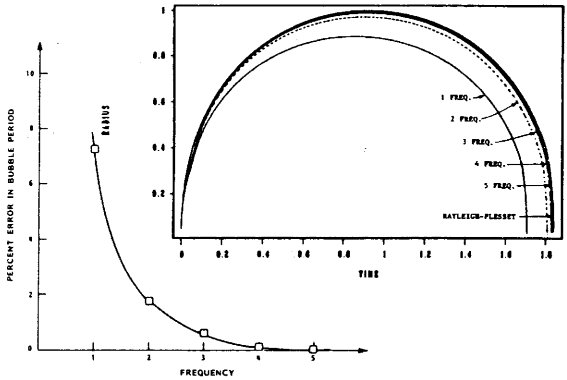

FIGURE 2. INFLUENCE OF MESH REFINEMENT ON ACCURACY. COMPARISON OF NORMALIZED SPHERICAL BUBBLE RADIUS VERSUS NORMALIZED TIME FOR VARIOUS DISCRETIZATION FREQUENCIES: f=1 (92 nodes), f=2 (42n), f=3 (92n), f=4 (162n), f=5 (252n). ALSO SHOWN IS THE PERCENT ERROR ON THE BUBBLE PERIOD.

The second series of comparisons was made with the previously studied axisymmetric cases available in the open literature, and have shown, as described below, differences with these studies of the order of 0.1 percent on the bubble period. Finally, comparison with actual test results of the complex three-dimensional case presented here, Figure 8, shows strikingly similar complex bubble shapes with a systematic error of 12 percent on the times which was proven to be related to the bubble period lengthening influence of the container walls on the experimental results (see Chahine et al.[9]).

Figure 3 shows the results of an axisymmetric case of bubble growth and collapse computed using the above described algorithm. It shows some general 3-D shapes and bubble profiles depicting the growth and collapse in a gravity field near an infinite horizontal plate above the bubble at a standoff ratio of $L/R_{max} = 1.50$, where L is the perpendicular distance from the initial bubble center to the plate. Here, the initial spherical bubble was discretized using 162 nodes resulting in 320 triangular panels. All coordinates have been normalized by R_{max} = 17cm. The figure shows how the bubble grows nearly spherically, then, during the collapse phase, flattens on the side which is opposite to the plate and forms a reentrant jet in a direction perpendicular to the plate. Note that for this case, the plate is located directly above the bubble, so both the buoyancy effects and the effects of the nearby boundary are in the same direction, vertically upward. The total period of the bubble, scaled by the Rayleigh time, $R_{max}/\sqrt{P/\rho}$ was about 2.084. P is the difference between the ambient pressure and the minimum bubble pressure. This agrees very well with the bubble period given by Blake, et al.[7] who report a value of approximately 2.097 for a similar case computed in the absence of gravity with their axisymmetric scheme and a larger number of panels. The maximum velocity attained by the jet in this simulation was $11.1\sqrt{P/\rho}$. This, too, compares very well with the results of other studies.

Figures 4 and 5 show fully the three-dimensional bubble growth and collapse when the infinite plate was moved to a vertical position adjacent to the bubble. The two cases were ran when the plate was at standoff ratios of L/R_{max} = 1.50, and 1.00. With gravity acting vertically downward, the two competing forces (gravity, presence of plate) are perpendicular, rather than parallel to each other. The same initial discretization is used.

Both of these figures show very clearly the formation of the reentrant jet moving at an angle upward toward the plate. Given that the two competing forces no longer act along the same line, one would expect that the jet would form in some resulting direction depending on the proximity of the plate. Comparison of the two figures shows that indeed this is the case. In Figure 4, where the bubble is initially closer to the plate, the reentrant jet appears to act along a line that is more nearly perpendicular to the plate. In Figure 4, the angle of the reentrant jet is more acute and the jet penetrates the bubble and touches the other side at a point much closer to the top of the bubble than for the bubble in Figure 5. Also one notices that, during the collapse, once the jet has touched the other side of the bubble, the bubble retains a larger volume for the case where the plate is closer. This has been demonstrated in the axisymmetric models and is very evident here as well. It is also apparent from the figures that the bubble growth is an important consideration. Deviation from sphericity, for instance, at maximum bubble size is observed and is larger when the bubble is initially closer to the plate. Bubble periods are noticeably changed by the wall configuration relative to gravity. Placing the boundary vertically rather than horizontally results in an increased normalized period from 2.084 to 2.101. Moving the bubble closer to the wall lengthens the period still more. This is consistent with the known lengthening effect of the boundary and the reduction in period caused by the buoyancy force.

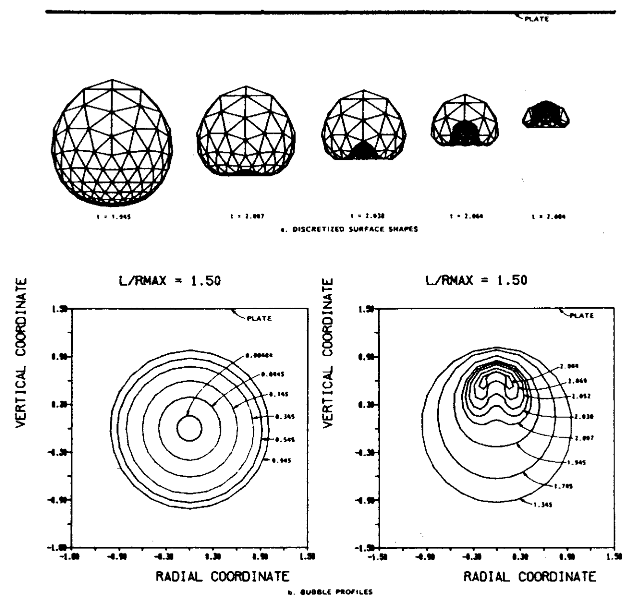

FIGURE 3 - AXISYMMETRIC BUBBLE GROWTH AND COLLAPSE.
L/R_{max} = 1.50, R_{max}/R_o = 17, P_{g_o}/P_a = 1500,
NORMALIZING RAYLEIGH TIME = 0.01453 sec.
R_{max} = 0.17m, P_{amb} = 20 psi

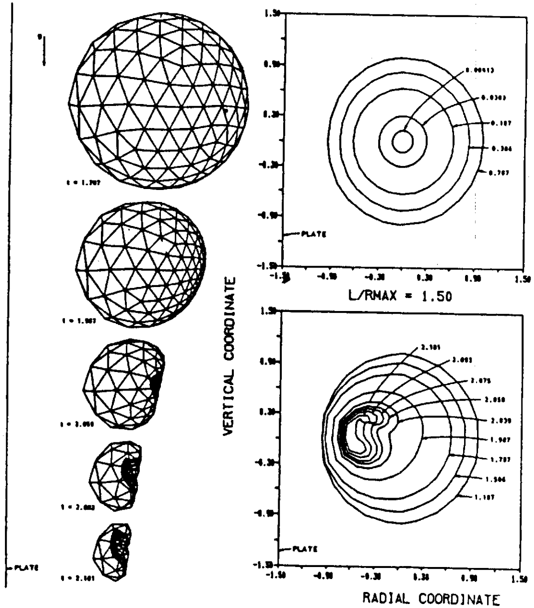

a. Surface Shapes

b. Bubble Profiles

FIGURE 4 - THREE-DIMENSIONAL BUBBLE GROWTH AND COLLAPSE. $L/R_{max} = 1.50$, $R_{max}/R_o = 17$, $P_{go}/P_a = 1500$, Normalizing Rayleigh Time = 0.01453sec. Vertical Wall.

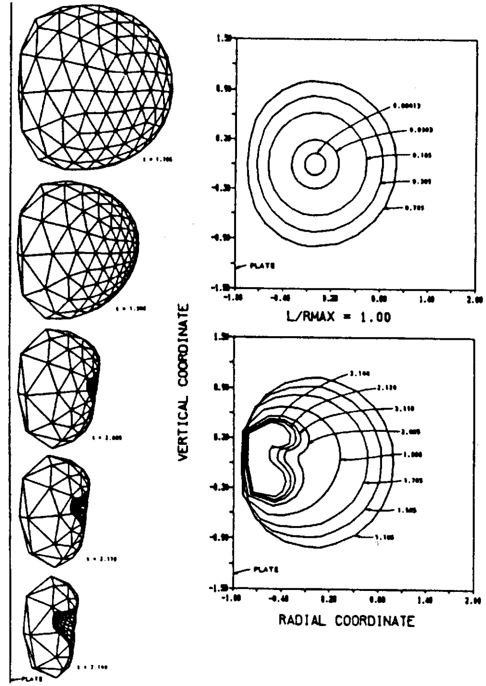

a. Surface Shapes

b. Bubble Profiles

FIGURE 5 - THREE-DIMENSIONAL BUBBLE GROWTH AND COLLAPSE. $L/R_{max} = 1.00$, $R_{max}/R_o = 17$, $P_{go}/P_a = 1500$, Normalizing Rayleigh Time = 0.01453sec. Vertical Wall.

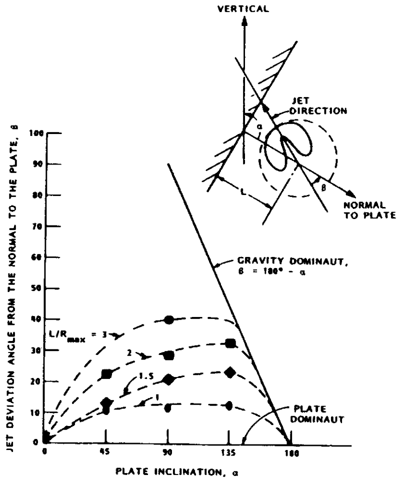

FIGURE 6 - RELATIVE EFFECTS OF GRAVITY FORCE AND PLATE PRESENCE ON REENTRANT JET ANGLE

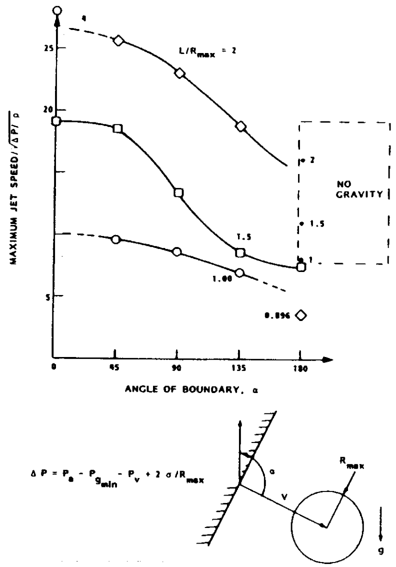

FIGURE 7 - INFLUENCE OF GRAVITY FORCE AND FLAT PLATE PRESENCE ON REENTRANT JET SPEED

Figures 6 and 7 summarize the results of a series of runs where the plate angle relative to gravity field and the plate standoff distance to the center of explosion have been varied. Figure 6 shows the deviation angle from the normal to the plate, β, versus the angle α between the plate normal and the vertical axis. The set of curves in the figure is for various values of $\bar{L}= L/R_{max}$. When $\bar{L}$ is very small, wall effect is predominant and the jet is practically normal to the plate, $\beta= 0$. β increases with $\bar{L}$ and attains a maximum when $\bar{L}$ goes to infinity. In that case, gravity forces are predominant and the reentrant jet is vertical directed upward independent of the plate angle α. However, with our definitions of α and β, the limit value of β depends on α as follows:

$$\beta_{limit} = 180° - \alpha \qquad (17)$$

For intermediate values of $\bar{L}$, the deviation angle from normal increases with α to attain a maximum for values of α between 90° and 135°. This result should not be generalized and is probably dependent on a Froude number based on the maximum bubble size, its period (or energy of the explosion) and the acceleration of gravity. The curves show a skewness toward higher α's, which reflects the fact that for $\alpha > 40°$, both gravity and plate presence act in the same direction, while for $\alpha < 90°$, these two forces act in opposite directions. (Note that $\alpha = 0°$ corresponds to a horizontal plate below the explosion center while $\alpha = 180°$ corresponds to a horizontal plate above the explosion center).

Figure 7 shows the influence of gravity and the proximity of the flat plate on the reentrant jet speed. Several important observations can be made form this figure.

a. The jet speed increases with distance from the plate.

b. The jet speed is higher when buoyancy forces and the plate presence do not act in the same direction.

c. The influence of plate angle on the jet speed is negligible both for very large and small values of $\bar{L}$.

d. The influence of α on the jet speed is the sharpest for $\bar{L} \sim 1.5$, limit value for which the jet direction changes sides for $\alpha = 180°$.

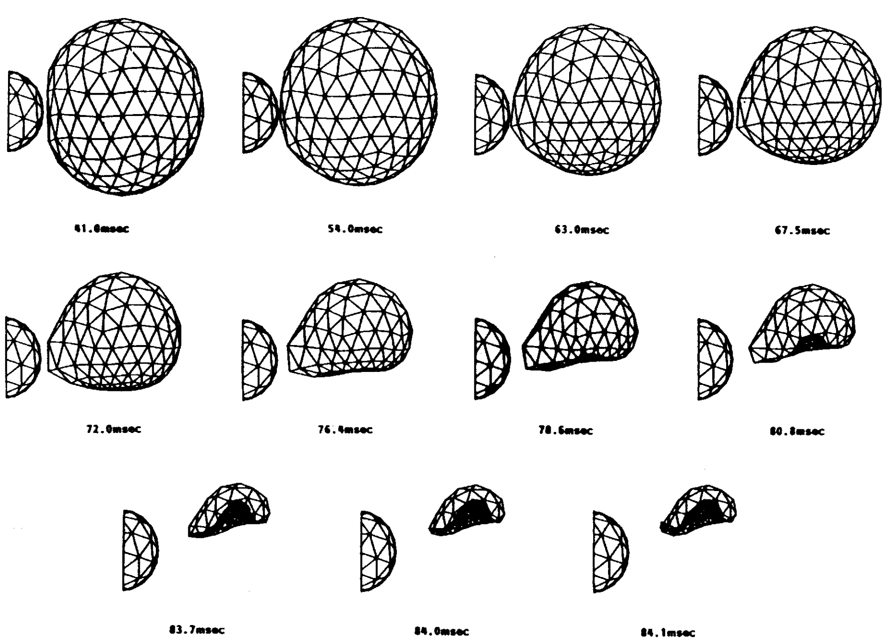

FIGURE 8 - BUBBLE COLLAPSE NEAR AXISYMMETRIC BODY
4 FREQUENCY DISCRETIZATION

Figure 8 shows the interaction between an unsteady bubble and an axisymmetric finite-size body. The center of the submerged body was placed at the same depth as the initial center of the bubble and at a distance to the axisymmetric body of 1.0 maximum bubble radii. Gravity was also included, so the two forces (buoyancy and body attraction) were acting perpendicularly to each other. The parameters for this case were chosen to match the experimental case shown in Figure 5 in Snay, Goertner and Price[11]. The computed bubble shapes closely resembles those actually recorded in the small scale underwater explosion test. A portion of the bubble is seen to adhere to the nearby body while the remainder behaves as if only gravity is the influencing factor. The one major discrepancy between the numerical and experimental results is the period of the growth and collapse of the bubble. The measured period is about 12 percent longer than the computed bubble period. This difference is mainly due to the fact that the experiments were conducted in a finite size cylindrical tank (diameter three times the maximum bubble diameter). The presence of the tank walls was shown by the numerical simulations to have a lengthening effect of the same order of magnitude on an otherwise isolated bubble.

This study is presently being extended to more accurately describe the latest phase of the bubble collapse when the reentrant jet approaches the opposite side of the bubble. Numerical instabilities occur in that last phase and can be reduced by smoothing techniques. Similarly, the pressures generated on the nearby plate become unsteady and need to be more accurately determined.

REFERENCES

1. J. R. Blake & D. C. Gibson, "Cavitation Bubbles Near Boundaries," *Ann. Rev. of Fl.Mech.*, **19**, 99-123, 1987.
2. M. S. Plesset & R. B. Chapman, "Collapse of a Vapor Cavity in the Neighborhood of a Solid Wall," *Cal. Tech. Rep.* 85-48, 1969.
3. A. Shima & K. Nakajima, "The Collapse of a Non-Hemispherical Bubble Attached to Solid Wall," *J. Fluid Mech.*, **80** (2), 369-391, 1977.
4. G. L. Chahine & A. G. Bovis, "Pressure Field Generated by Nonspherical Bubble Collapse," *J. Fluids Eng.*, **105** (3), 356-364, September 1983.
5. G. L. Chahine & H. L. Liu, "A singular perturbation Theory of the Growth of a Bubble Cluster in a Superheated Liquid," *J. Fluid Mech.*, **156**, 257-279, 1985.
6. L. Guerri, G. Lucca & A. Prosperetti, "A Numerical Method for the Dynamics of Non-Spherical Cavitation Bubbles," **Proc. 2nd Int. Coll. on Drops and Bubbles**, JPL Publication 82-7, Monterey CA, Nov 1981.
7. J. R. Blake, B. B. Taib, & G. Doherty, "Transient Cavities Near Boundaries," *J. Fluid Mech.*, **170**, 479-497, 1986.
8. T. O. Perdue, "A Three-Dimensional Numerical Simulation of Bubble Growth and Collapse Near a Rigid Boundary in the Presence of Gravity," M.S. Thesis, University of Maryland, 1988.
9. G. L. Chahine, T. O. Perdue, & C. B. Tucker, "Interaction Between an Underwater Explosion Bubble and a Solid Submerged Structure," Tracor Hydronautics Technical Report 86029-1, April 1988.
10. G. L. Chahine, "Experimental and Asymptotic Study of Nonspherical Bubble Collapse," *Appl. Sci. Res.*, **38**, 187-197, 1982.
11. H. G. Snay, J. F. Goertner & R. S. Price, "Small Scale Experiments to Determine Migration of Explosion Gas Globes Towards Submarines," Navord Report 2280, July 1952.

FIGURE CAPTIONS

Figure 1. Normalized oblique coordinates ζ, η on panel ABC.

Figure 2. Influence of mesh refinement on accuracy. Comparison of normalized spherical bubble radius versus normalized time for various discretization frequencies: f = 1 (92 nodes), f = 2 (42n), f = 3 (92n), f = 4 (162n), f = 5 (252n). Also shown is the percent error on the bubble period.

Figure 3. Axisymmetric bubble growth and collapse. L/R_{max} = 1.50, R_{max}/R_o = 17, P_{g_o}/P_a =1500. Normalizing Rayleigh time = 0.01453 sec. R_{max} = 0.17m, $P_{amb} \cong$ 20 psi.

3a. Discretized surface shapes

3b Bubble profiles

Figure 4. Three-dimensional bubble growth and collapse, L/R_{max} = 1.50, R_{max}/R_o = 17, P_{g_o}/P_a = 1500. Normalizing Rayleigh time = 0.01453 sec. Vertical wall.

Figure 5. Three-dimensional bubble growth and collapse, L/R_{max} = 1.00, R_{max}/R_o = 17, P_{g_o}/P_a =1500. Normalizing Rayleigh time = 0.01453 sec. Vertical wall.

Figure 6 Relative effects of gravity force and plate presence on re-entrant jet angle.

Figure 7. Influence of gravity force and flat plate presence on re-entrant jet speed.

Figure 8. Bubble collapse near axisymmetric body 4-frequency discretization.